

Milky Way demographics with the VVV survey^{***}

I. The 84-million star colour-magnitude diagram of the Galactic bulge

R. K. Saito^{1,2,3}, D. Minniti^{1,3,4}, B. Dias⁵, M. Hempel^{1,3}, M. Rejkuba⁶, J. Alonso-García^{1,3}, B. Barbuy⁵, M. Catelan^{1,3},
J. P. Emerson⁷, O. A. Gonzalez⁶, P. W. Lucas⁸, and M. Zoccali^{1,3}

¹ Departamento de Astronomía y Astrofísica, Pontificia Universidad Católica de Chile, Vicuña Mackenna 4860, Casilla 306, Santiago 22, Chile

² Departamento de Física y Astronomía, Facultad de Ciencias, Universidad de Valparaíso, Ave. Gran Bretaña 1111, Playa Ancha, Casilla 5030, Valparaíso, Chile

³ The Milky Way Millennium Nucleus, Av. Vicuña Mackenna 4860, 782-0436 Macul, Santiago, Chile

⁴ Vatican Observatory, Vatican City State V-00120, Italy

⁵ Universidade de São Paulo, IAG, Rua do Matão 1226, Cidade Universitária, São Paulo, 05508-900, Brazil

⁶ European Southern Observatory, Karl-Schwarzschild-Strasse 2, D-85748 Garching, Germany

⁷ Astronomy Unit, School of Physics and Astronomy, Queen Mary University of London, Mile End Road, London, E1 4NS, UK

⁸ Centre for Astrophysics Research, University of Hertfordshire, College Lane, Hatfield AL10 9AB, UK

Received January 01, 2000; accepted January 01, 2000

ABSTRACT

Context. The Milky Way (MW) bulge is a fundamental Galactic component for understanding the formation and evolution of galaxies, in particular our own. The ESO Public Survey VISTA Variables in the Vía Láctea is a deep near-IR survey mapping the Galactic bulge and southern plane. Particularly for the bulge area, VVV is covering $\sim 315 \text{ deg}^2$. Data taken during 2010 and 2011 covered the entire bulge area in the JHK_s bands.

Aims. We used VVV data for the whole bulge area as a single and homogeneous data set to build for the first time a single colour-magnitude diagram (CMD) for the entire Galactic bulge.

Methods. Photometric data in the JHK_s bands were combined to produce a single and huge data set containing 173, 150, 467 sources in the three bands, for the $\sim 315 \text{ deg}^2$ covered by VVV in the bulge. Selecting only the data points flagged as stellar, the total number of sources is 84, 095, 284.

Results. We built the largest colour-magnitude diagrams published up to date, containing 173.1+ million sources for all data points, and more than 84.0 million sources accounting for the stellar sources only. The CMD has a complex shape, mostly owing to the complexity of the stellar population and the effects of extinction and reddening towards the Galactic centre. The red clump (RC) giants are seen double in magnitude at $b \sim -8^\circ - 10^\circ$, while in the inner part ($b \sim -3^\circ$) they appear to be spreading in colour, or even splitting into a secondary peak. Stellar population models show the predominance of main-sequence and giant stars. The analysis of the outermost bulge area reveals a well-defined sequence of late K and M dwarfs, seen at $(J - K_s) \sim 0.7 - 0.9 \text{ mag}$ and $K_s \geq 14 \text{ mag}$.

Conclusions. The interpretation of the CMD yields important information about the MW bulge, showing the fingerprint of its structure and content. We report a well-defined red dwarf sequence in the outermost bulge, which is important for the planetary transit searches of VVV. The double RC in magnitude seen in the outer bulge is the signature of the X-shaped MW bulge, while the spreading of the RC in colour, and even its splitting into a secondary peak, are caused by reddening effects. The region around the Galactic centre is harder to interpret because it is strongly affected by reddening and extinction.

Key words. Galaxy: bulge – Galaxy: center – Galaxy: structure – Galaxy: stellar content – Surveys

1. Introduction

The bulge of the Milky Way (MW) is a fundamental Galactic component for understanding the formation and evolution not only of our Galaxy, but of galaxies in general. In the MW the stars can be individually resolved down to faint magnitudes, allowing a complete understanding of its structure, age, kinematics, and chemical composition. However, because the bulge and plane concentrate not only most of the stars in the MW, but also gas and dust, observations of the Galactic cen-

tre are difficult because they are affected by crowding and extinction. Optical surveys such as MACHO (Alcock et al. 1999) and OGLE (Udalski et al. 1993) are highly affected by extinction while past near-infrared (near-IR) surveys such as 2MASS are limited to bright sources ($K_s \sim 14.3 \text{ mag}$; Skrutskie et al. 2006), and do not allow a complete view of the bulge populations.

The new ESO Public Survey VISTA Variables in the Vía Láctea (VVV) is a deep near-IR survey mapping 562 square degrees in the southern plane and bulge of our Galaxy (Minniti et al. 2010). Particularly for the bulge area, VVV is covering $\sim 315 \text{ deg}^2$. The VVV survey observes in five near-IR passbands ($ZYJHK_s$), where extinction effects are lower than in the optical wavelengths, and it is much deeper than previous near-IR surveys. The 5σ limiting magnitude of the VVV data using aperture photometry is $K_s \sim 18.5 \text{ mag}$ in clean

Send offprint requests to: R. K. Saito: rsaito@astro.puc.cl

* Based on observations taken within the ESO VISTA Public Survey VVV, Programme ID 179.B-2002.

** The VVV survey data are available through the ESO archive <http://www.eso.org/sci/archive.html>

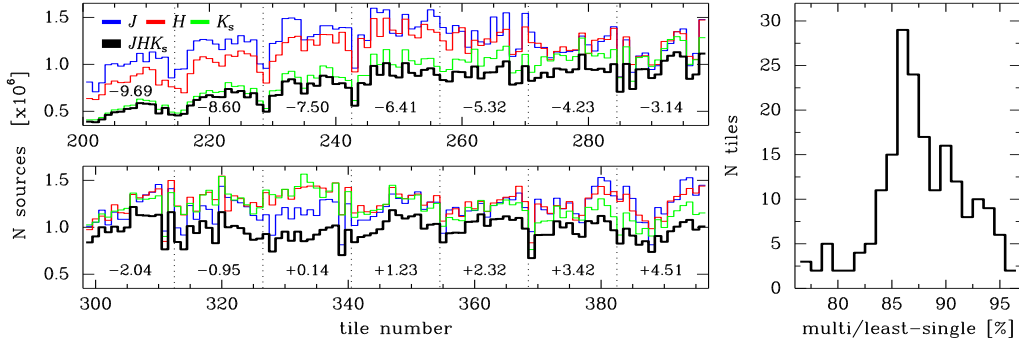


Fig. 1. Left-hand panels: total number of sources present in the J , H , and K_s singleband and in the JHK_s multi-band catalogue for each VVV bulge tile. The tiles are numbered from b201 to b396, starting at the bottom-left corner of the VVV bulge area ($l, b = -10, -10$). The Galactic latitude for the tile centres is shown in the figure, while dashed lines mark the edge of each line of tiles across the bulge. The right-hand panel presents a histogram with the ratio between the number of sources in the multi-band catalogue in relation to its least numerous single-band catalogue.

fields, which allows one to monitor bright sources such as RR Lyrae and clump giants stars along the whole Galactic bulge and plane, solar-type stars at the Galactic centre distances, and even faint dwarf stars a few kpc away. The VVV data reach the main-sequence turn-off (MSTO) even in intermediate- to high-extinction areas ($E(B - V) \lesssim 4.0$, Minniti et al. 2010).

The VVV photometry for the whole bulge area was combined into a single, huge, and homogeneous data set, allowing us to build for the first time a single colour-magnitude diagram for the entire Galactic bulge ($\sim 315 \text{ deg}^2$). Here we present the 84-million star VVV colour-magnitude diagram (CMD) for the Galactic bulge. This is the largest CMD ever published for a large homogeneous data set, a significant step forward since the publication of the 9-million star CMD of the Large Magellanic Cloud (Alcock et al. 2000). We discuss the differences in the morphology caused by crowding, extinction and sky brightness. A forthcoming paper will present a similar analysis for the populations across the VVV Galactic plane area.

2. Observational data and catalogues

The VVV is an ESO Public Survey scanning the MW bulge and plane with the 4-m class VISTA Telescope (Minniti et al. 2010). The total observed area is about 562 deg^2 , within $-10.0^\circ \lesssim l \lesssim +10.5^\circ$ and $-10.3^\circ \lesssim b \lesssim +5.1^\circ$ in the bulge, and within $294.7^\circ \lesssim l \lesssim 350.0^\circ$ and $-2.25^\circ \lesssim b \lesssim +2.25^\circ$ in the plane. The VVV survey observes in five passbands, namely Z ($0.87 \mu\text{m}$), Y ($1.02 \mu\text{m}$), J ($1.25 \mu\text{m}$), H ($1.64 \mu\text{m}$), and K_s ($2.14 \mu\text{m}$) bands, and also conducts a variability campaign in K_s -band only, with ~ 100 pointings spanning five years (2010–2014).

Each unit of VISTA observations is called a (filled) “tile”, consisting of six individual (unfilled) pointings (or “pawprints”) and covers a 1.64 deg^2 field of view. To fill up the VVV area, a total of 348 tiles are used, with 196 tiles covering the bulge (a 14×14 grid) and 152 for the Galactic plane (a 4×38 grid).

The schedule for the first year (2010) comprised the observation of the whole VVV plane and bulge areas in the five passbands, as well as five complementary epochs in K_s -band. However, delays during the campaign prevented the completion of the planned observations, with some of the first year data being observed during 2011.

The delays mostly affected the Z and Y observations and the variability campaign, while the JHK_s observations were fully completed during the first semester of 2011. From the 196 pointings needed to cover the total bulge area, 180 were completed and made publicly available with the VVV Data Release 1 (DR1) on August 2011 (a comprehensive description of this dataset is given by Saito et al. 2012). The present work is based on J , H and K_s photometry, from the VVV DR1 and DR2 data (in preparation), with complete bulge coverage in the three bands.

Photometric catalogues for the VVV images are provided by the Cambridge Astronomical Survey Unit (CASU)¹. The catalogues contain the positions, fluxes, and some shape measurements obtained from different apertures, with a flag indicating the most probable morphological classification. In particular, we note that “-1” is used to denote the best-quality photometry of stellar objects. Some other flags are “-2” (borderline stellar), “0” (noise), “+1” (non-stellar objects), “-7” (sources containing bad pixels), and “-9” (saturated sources). Our entire analysis was performed using the *apermag3* aperture fluxes, which are used in the CASU catalogues and in the VISTA Science Archive (VSA)² as the default values to represent the flux. However, we note that the CASU pipeline starts to measure the positions and fluxes with the *apermag1* ($1''$ diameter) and then successively increases the aperture by a factor of $\sqrt{2}$ in diameter. For highly crowded fields as in the inner Galactic bulge, using *apermag1* and *apermag2* can be more suitable than *apermag3*.

The VVV data are in the natural VISTA Vegamag system, with the photometric calibration in JHK_s performed using the VISTA magnitudes of unsaturated 2MASS stars present in the images. A final tile catalogue comprises the photometry for an area of $\sim 1.64 \text{ deg}^2$ in the sky, with the total number of point sources found in each single-band catalogue ranging from 408, 858 at the outermost bulge region (tile b202, K_s -band) to 1, 597, 046 sources per tile at the innermost Galactic centre (tile b246, J -band). The K_s -band catalogues are shallower than J and H at high Galactic latitudes, while near the Galactic plane ($|b| \lesssim 3 \text{ deg}$) the three catalogues present a similar number of sources for most tiles (see Fig. 1). On the Galactic plane the

¹ <http://casu.ast.cam.ac.uk/vistasp/>

² <http://horus.roe.ac.uk/vsa/index.html>

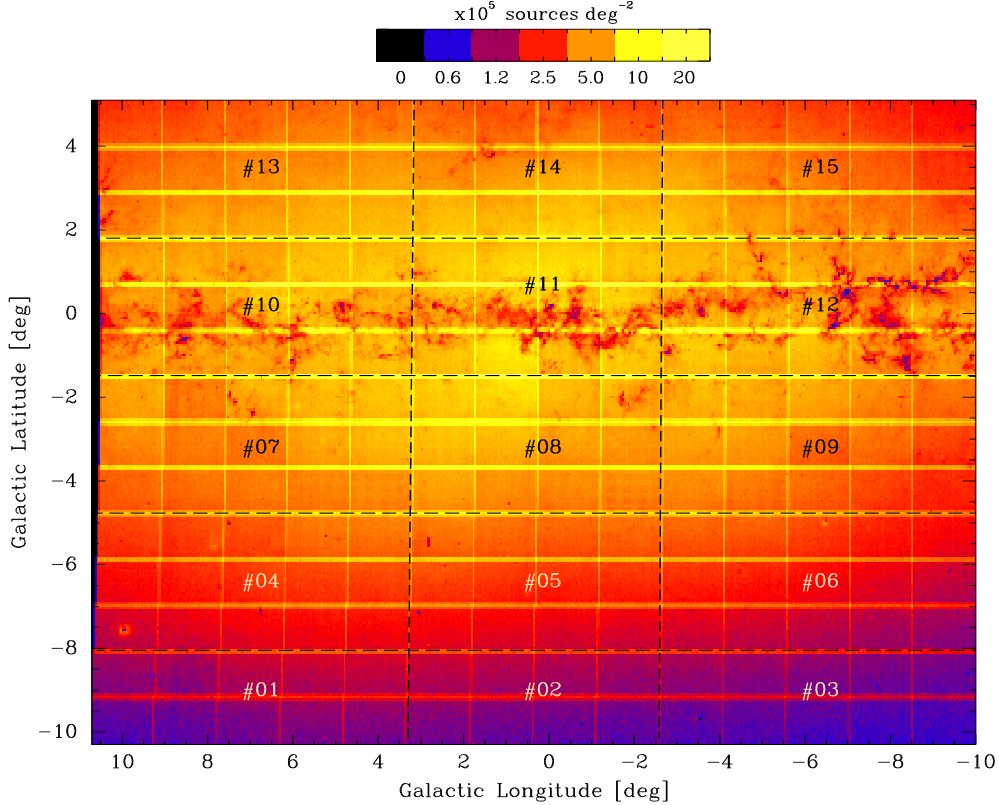


Fig. 2. Density plot in logarithmic scale showing the VVV bulge area. The map was made using the multi-band JHK_s CASU v1.1 and v1.2 catalogues for point sources brighter than $K_s = 16.5$ mag (see text). Crowded areas appear in yellow, while less populated regions as well as highly extinguished areas are shown in blue. The overlapping regions between the tiles are highlighted since the point sources are accounted for twice. Dashed lines mark the 15 areas selected to build the colour-magnitude diagrams shown in Fig. 6 (see Section 4). The source density, in units of 10^5 sources deg^{-2} , is indicated in the horizontal bar at the top.

high extinction mostly affects the J - and H -band, which renders the K_s -band catalogue the one with the most entries among the three bands.

The comparison between the source counts of different tile catalogues depends strongly, but not exclusively, on their position with respect to the stellar crowding, i.e., the detection rate for tiles at high Galactic latitude will be significantly higher than for a tile in the Galactic plane. This effect becomes even more important for the aperture-photometry-based source catalogues used in this study. Artificial star experiments carried out on subsections of two different tiles in the bulge area (b204 and b314, respectively, see Saito et al. 2012) show that the single-band tile catalogues are 80% complete down to $K_s \sim 17.0$ in the outermost bulge region (b204), but in the innermost bulge (b314) the same percentage is reached at $K_s \sim 15.5$.

The single-band CASU catalogues for each tile were matched by VVV team members, with most of sources matched within $\leq 0''.5$, as expected from the astrometric accuracy of the VVV data (Saito et al. 2012). For a couple of tiles the ellipticity sometimes varies between the filters, hence sources appear as high-quality stars in one filter but are rejected in another, or appear with a distinct morphological classification. Therefore, some sources are lost during the matching procedure. For most tiles the multi-band catalogues contain more than 85% of the total sources found in the least numerous singleband catalogue used for the matching (see Fig. 1). The performance is maximum

at high Galactic latitude, with the multi-band catalogues reaching up to $\sim 96\%$ of successful matches. On the other hand, the increasing source confusion and extinction towards the Galactic centre reduces the number of matches in the innermost region ($|b| < 1$ deg), with a few tiles showing $\sim 75\text{--}80\%$ of the total sources present in the least numerous singleband catalogue. Some larger “steps” seen between adjacent tiles in Fig. 1 are caused not only by differences in the quality and deepness of data, but also by the obscured regions at lower Galactic latitudes. There are 173, 150, 467 sources in all multi-band catalogues for the 196 bulge tiles.

Figure 2 shows the VVV bulge area as a density map corresponding to the mosaic of all multi-band catalogues. To equalize the increasing sky brightness towards the Galactic centre that is generated by the contribution of the underlying, unresolved faint stars, a cut in $K_s = 16.5$ mag was applied in the catalogues, with a total of 128,660,076 sources remaining in the map. High-density areas appear in yellow, while less populated regions and high-extinction areas are shown in blue. The tiling pattern produces overlapping regions between the tiles. These are highlighted in the map, since the point sources in these regions are counted twice. The overlapping area has been used by the VVV team to check the photometric and astrometric accuracy, but it was not been coadded.

In a few cases the colour pattern (or source density) changes between adjacent tiles, because some sources in lower quality

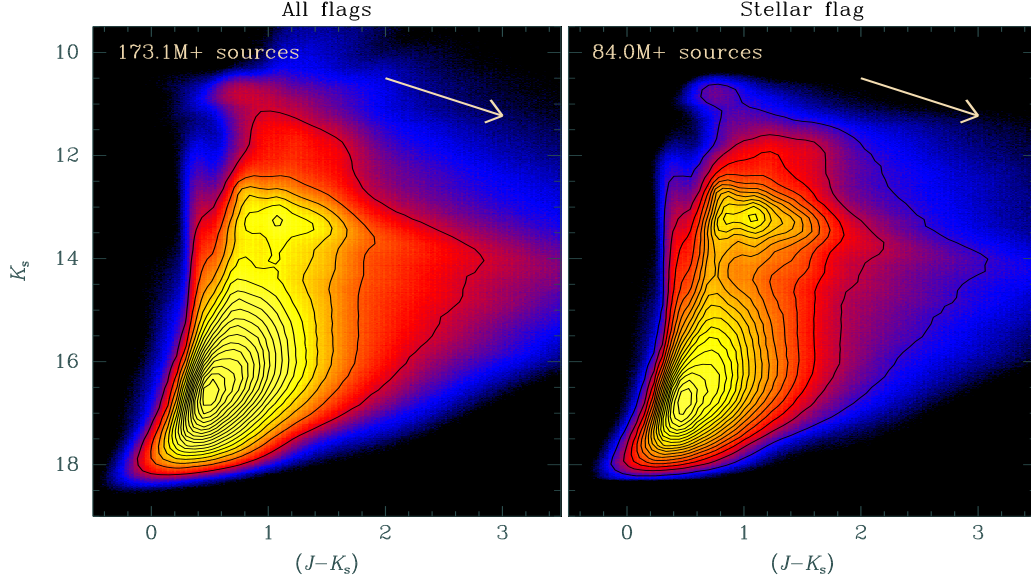


Fig. 3. $K_s \times (J - K_s)$ colour-magnitude diagram for the VVV bulge area, as shown in Fig. 2. In the left-hand panel is the CMD for all point sources found in the matched catalogues, in a total of 173, 150, 467 sources. The right-hand panel shows only point sources flagged as “stellar” in the three J , H , and K_s catalogues, according with the CASU photometry. The total number of stellar sources is 84, 095, 284. Contour lines mark density levels in steps of 5% from the maximum density. The reddening vector associated with an extinction of $E(B - V) = 2$, based on the relative extinctions of the VISTA filters, and assuming the Cardelli et al. (1989) extinction law, is also shown in both panels.

Table 1. Effective wavelengths for the VISTA filter set used in the VVV observations and the relative extinction for each filter based on the Cardelli et al. (1989) extinction law (from Catelan et al. 2011).

Filter	$\lambda_{\text{eff}}(\mu\text{m})$	A_X/A_V	$A_X/E(B - V)$
J	1.254	0.280	0.866
H	1.646	0.184	0.567
K_s	2.149	0.118	0.364

images were rejected, as cited above. This effect is mostly seen near the Galactic centre, where the detection rate is more affected by crowding. Several tiny dark spots seen in the map mark the regions with no detections around bright, saturated stars. The globular cluster M22 is also detected at $l, b \sim +9.9, -7.5$. It appears as a region with increasing density, which suddenly drops to a spot with no detections, due to confusion of the aperture photometry in detecting sources in highly populated fields such as globular cluster cores.

3. The 84-million star CMD

We used the JHK_s VVV multiband catalogues of the complete bulge as a single data set to build the largest colour-magnitude diagrams published to date. The left-hand panel of Fig. 3 shows the CMD containing 173, 150, 467 sources for the $\sim 315 \text{ deg}^2$ area covered by VVV in the bulge. It contains all sources found in the catalogues and it is shown as a density plot with contour curves marking the same star density levels in steps of 5% from the maximum intensity. The CMD shows the same

data as in Fig. 2, but also includes the point sources fainter than $K_s = 16.5 \text{ mag}$, in contrast with the additional selection criteria applied in Fig. 2. The brightest stellar sources appear at $K_s \sim 9.9 \text{ mag}$, while the 5σ limiting magnitude depends strongly on crowding. In the outer bulge the limiting magnitude is $K_s \sim 18.3 \text{ mag}$, but at the Galactic centre the presence of underlying, unresolved faint stars contributes to increase the sky brightness, which limits the photometry to $K_s \sim 16.3 \text{ mag}$. A small fraction of the sources, flagged as “saturated stars” and “noise”, appears to be populating the upper and lower limits of the CMD, respectively.

The right-hand panel of Fig. 3 shows the CMD built only with the data points flagged as “-1”, stellar sources, in the J , H , and K_s catalogues, in a total of 84, 095, 284. Since the stellar flag comprises only best-photometry data points, structures are clearer seen in the right-hand panel of Fig. 3. Moreover, the limiting magnitude is shallower, since the faint sources flagged as “noise” are not present. Fig. 3 also shows in both panels the reddening vector associated with an extinction of $E(B - V) = 2$, based on the relative extinctions of the VISTA filters using the Cardelli et al. (1989) extinction law (see Table 1). However, we notice that the reddening law varies significantly in the innermost regions of the MW (e.g., Nishiyama et al. 2009).

Because the CMDs were created by combining all individual 196 tile catalogues, they include the overlapping regions between the tiles, which comprise $\sim 7\%$ of the total point sources. Thus, $\sim 12.6\text{M}$ of the 173.1M sources are counted twice, which reduces the number of unique sources to $\sim 160.4\text{M}$. Similarly, $\sim 78.0\text{M}$ of the 84.1M stellar sources are unique. The overlapping areas are equally spaced along the bulge in both l and b directions, and therefore do not contribute any bias or special trend in magnitude or colour.

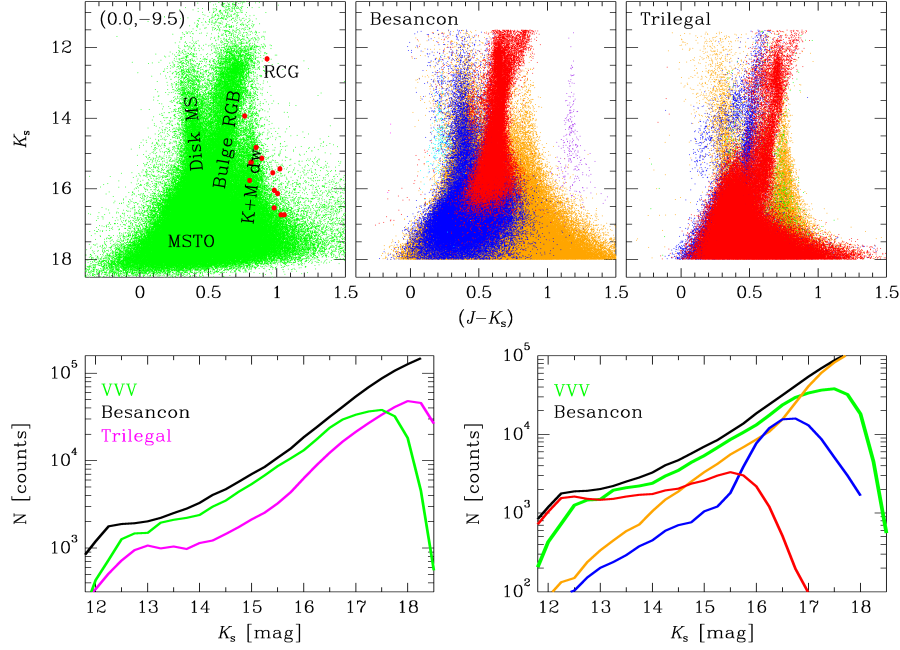


Fig. 4. Top-left panel: $K_s \times (J - K_s)$ CMD for an area of 1 sq. deg. centred at $(l, b) = (0.0, -9.5)$. This is the outermost region in the VVV bulge area, on the Galactic minor axis. The different stellar populations are labelled. Red circles show the colours of M-dwarfs for a distance modulus of $(m_{K_s} - M_{K_s}) = 7$ mag (see text). The top-central and top-right panels show stellar population synthesis models of the Galaxy for the same region, provided by the Besançon (centre) and Trilegal models (right-hand), including photometric errors and an extinction as described in the text (see Section 4). In the Besançon model stars are shown according to luminosity class. Main-sequence stars are depicted in orange, subgiants in blue and giants are red dots. Supergiants, bright giants, and white dwarfs are also present, but there are only a few (show in light blue, magenta and purple, respectively). The relative numbers are given in Table 3. On the other hand, the Trilegal model highlights the Galactic components, with 69.6% of the stars belonging the bulge (in red), 18.3% are located in the halo (in blue) and 10.6% are thin-disk stars (in orange). A small fraction of 1.5% are thick-disk stars (green dots). The bottom-left panel shows the luminosity function for data and model. The bottom-right panel shows the luminosity function of each luminosity class in the Besançon data. The colour code is the same as used in the CMDs.

The following description, and the next sections discuss the high-quality CMD that presents the stellar sources.

The VVV Bulge CMD has a complex shape, mostly because of the complexity of the stellar population, seen at different ranges of magnitudes and colours, and the effects of extinction and reddening towards the Galactic centre. Reddening affects the bulge populations at different levels, spanning from $E(B - V) \lesssim 0.2$ at $b \sim -10^\circ$, and up to $E(B - V) \sim 10$ at the Galactic centre (Gonzalez et al. 2012). Moreover, the reddening law changes in the innermost bulge regions, as cited above.

In particular, the red giant branch (RGB) is seen to be broader, with the main peak of the red clump (RC) giants at $(J - K_s), K_s \sim 1.05, 13.20$. The RC giants have structures ranging in colour and magnitude, with a secondary peak in colour at $(J - K_s), K_s \sim 0.85, 13.20$, and an elongated structure in magnitude with $\Delta K_s \sim 1$ mag. Those are caused mostly by the X-shaped bulge of the MW, producing the structure in magnitude, and by differential extinction, resulting in multiple structures in colour (see Section 5.1). The colour of the RGB stars is also affected by changes in the metallicity, which shows a gradient along the bulge minor axis (Zoccali et al. 2008). However, the effect is minimized in the RC, since the colour of RC giants is less affected by age and metallicity (e.g., Salaris & Girardi 2002).

4. Comparison with models

In this section we compare our data with stellar population synthesis models provided by the Besançon³ (Robin et al. 2003) and the Trilegal⁴ (Girardi et al. 2005) codes.

For the comparison we selected three regions of $1^\circ \times 1^\circ$ along the bulge. The first region is at high Galactic latitude, centred at $(l, b) = (0.0, -9.5)$. This is the outermost region of the VVV bulge area, and is the least crowded as well as least affected by reddening on the bulge minor axis, with $A_{K_s} = 0.023 \pm 0.010$ (see Table 2). Owing to these conditions its stellar population is well defined, allowing a better comparison with models.

The other two selected regions are centred at $(l, b) = (0.0, -6.0)$ and $(l, b) = (0.0, -3.0)$. These regions are highly affected by reddening and crowding, and are useful for testing the differences in the morphology of the CMDs. The mean values of reddening and extinction for each region are given in Table 2.

To properly account for the differential reddening across the 1 sq. deg. regions, we divided each region into 16 small areas of $15' \times 15'$ side. The mean A_{K_s} , $E(J - K_s)$, and respective A_V were calculated for each area using the reddening maps of

³ <http://model.obs-besancon.fr/>

⁴ http://stev.oapd.inaf.it/cgi-bin/trilegal_1.5

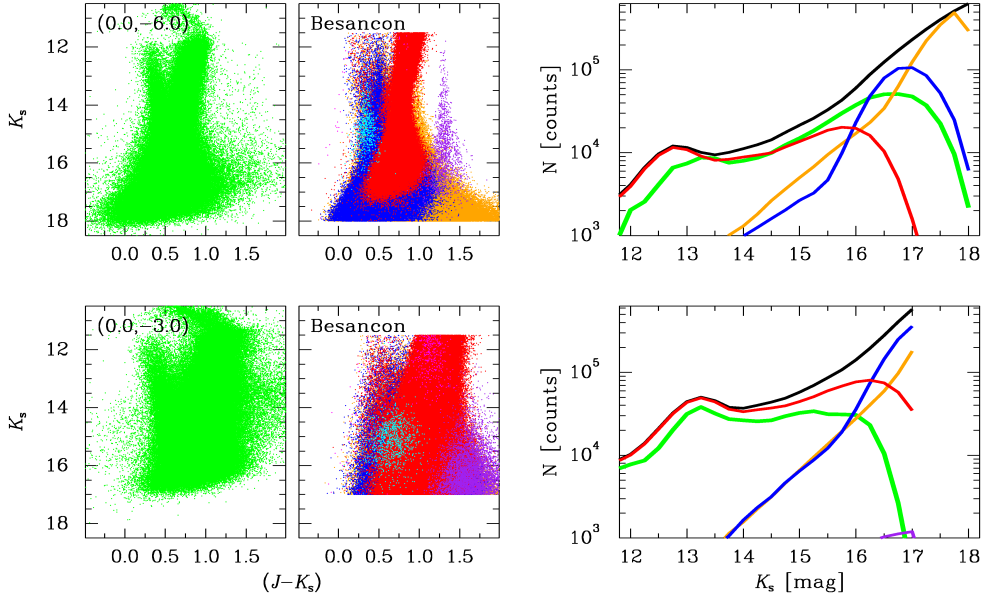


Fig. 5. Comparison between VVV and synthetic data provided by the Besançon model for the areas at $(l, b) = (0.0, -6.0)$ (top), and $(l, b) = (0.0, -3.0)$ (bottom). The notation is similar to that presented in Fig. 4.

Table 2. Mean values for the extinction and reddening for each 1 sq. deg. region provided by Gonzalez et al. (2012) using the Cardelli et al. (1989) extinction law.

(l, b) [deg]	A_{K_s}	$E(J - K_s)$	A_V
(0.0, -9.5)	0.023 ± 0.010	0.033 ± 0.014	0.194 ± 0.083
(0.0, -6.0)	0.110 ± 0.014	0.160 ± 0.020	0.932 ± 0.119
(0.0, -3.0)	0.320 ± 0.052	0.464 ± 0.075	2.710 ± 0.438

Gonzalez et al. (2012), and the Cardelli et al. (1989) extinction law. These values were used as input while querying the models for the synthetic data of each $15' \times 15'$ area. Finally, the data generated by the models for each 16 small areas were combined into a single data set corresponding to the entire 1 sq. deg. This procedure ensures that the spatial distribution of sources across the region and the changes in the reddening are well-accounted for the synthetic data.

The Trilegal model is available in the VISTA JHK_s colours, while the Besançon model uses the JHK system. Although our data use the VISTA system, the systems are sufficiently close that a comparison is useful for the conclusions. When synthetic Besançon models become available in the VISTA system, these should be used instead. The synthetic data were collected using the default parameters presented in both models, which include all luminosity classes belonging the four Galactic populations (thin disk, thick disk, halo and bulge) at the given line of sight, photometric errors, and extinction as described above. While the Besançon data output labels the sources according to the luminosity class, the Trilegal model complements the analysis because it classifies the sources according to the Galactic component.

The top-left panel of Fig. 4 shows the $K_s \times (J - K_s)$ CMD for the 1 sq. deg area at $(l, b) = (0.0, -9.5)$, with labels indicating the distribution of the stellar content. For quantitative purposes, the data include not only the stellar sources, but all unsaturated sources presented in the JHK_s multi-band catalogue. The CMDs built with Besançon and Trilegal data are shown in the top-central and top-right panels of Fig. 4, respectively. Complementary K_s luminosity functions are also shown in Fig. 4. In the bottom-left panel we present the luminosity function of all sources in each model, compared with the VVV data. The luminosity functions are quite similar, but the Besançon data are most numerous than VVV (+37% sources in the range $13 < K_s < 17$), while Trilegal delivers less stars than the real data (-49% in the same K_s range). This discrepancy in total numbers is expected because models based their calibration on data with different levels of completeness in the magnitude range of the VVV data (e.g., 2MASS, DENIS, OGLE, etc). However, the difference in the number of sources between VVV and the Besançon luminosity function entirely agrees with the results of our completeness tests performed on the VVV data in this region (see Section 2). The bottom-right panel of Fig. 4 presents the luminosity function of the Besançon data separately for each luminosity class.

We notice that the double-peaked RC is not modelled by the synthetic data and therefore does not allows a direct comparison. A recent paper by the Besançon team discuss the modeling of the double clump by introducing of a flaring bar in the current version of the Besançon code, see Robin et al. (2012). However, since they compared the model with 2MASS data, which are not complete at the fainter magnitude of the second clump, additional modifications in the model based on deep near-IR data are necessary (e.g., VVV and UKIDSS-GPS).

The Besançon model represents the VVV data well, showing the disk and bulge sequences at similar colour and magnitudes, as well the similar scattering at lower magnitudes due to the large

Table 3. Relative number of each luminosity class in the synthetic data provided by the Besançon model. The range in K_s was defined according to the limiting magnitude of the VVV data in each region.

(l, b) [deg] K_s range [mag]	Luminosity classes (relative number [%])		
	(0.0, -9.5) 11.5 – 18.0	(0.0, -6.0) 11.5 – 18.0	(0.0, -3.0) 11.5 – 17.0
Main-sequence	76.9	67.7	17.8
Subgiants	16.5	22.7	35.9
Giants	6.5	9.5	45.9
Supergiants	0.04	0.02	0.05
White dwarfs	0.05	0.06	0.3
Bright giants	<0.001	0.001	0.02

photometric errors. Main-sequence stars and subgiants are the most numerous sources, accounting for 76.9% and 16.5% of the total number, respectively. Giants account for 6.5%, but dominate the CMD for $K_s < 14$ mag. A small fraction of luminous supergiants, bright giants and white dwarfs is also present. Table 3 summarises the relative number of each luminosity class in the Besançon data. Finally, the top-right panel of Fig. 4 shows the CMD for the Trilegal data. The sources are labelled according to their Galactic components, which are distributed as follows. The bulge population is predominant with 69% of the total sources. Halo stars from farther out, behind the bulge, account for 19.6%, while the thin disk contributes 10%. Thick disk stars make up 1.4% of the total.

The comparison of our data with the models for the region at $(l, b) = (0.0, -9.5)$ allows us to conclude that (i) the MSTO highlighted in the VVV CMD is composed of bulge, halo and thin-disk stars, with a majority of main-sequence stars, but with a small fraction of subgiants. (ii) The sequence labelled at the left side as main-sequence (MS) stars is composed of subgiants and main-sequence stars from the thin disk. (iii) The bulge RGB at the right side is composed of giants from the bulge, but also includes a small fraction of halo stars behind the bulge. (iv) Finally, a sequence seen at the right-most side is comprised of late dwarfs belonging to the thin-disk.

Fig. 5 shows the VVV data compared with the synthetic data from the Besançon model for the regions at $(l, b) = (0.0, -6.0)$ and $(l, b) = (0.0, -3.0)$. The increasing crowding and reddening towards the Galactic centre introduces degeneracies both in magnitude and colours, that is why at $b = -3.0$ most of the sequences are seen overlaid. The relative number of each luminosity class also changes, not only due to intrinsic changes in the stellar content, but also because the increasing limiting magnitude of the VVV data that contribute to reduce the number of faint sources. While the number of main-sequence and subgiants decreases towards the Galactic centre, the bulge giants dominate the CMD at the inner bulge, increasing by a factor ~ 8 from the CMD at $b = -9.5$ (6.5% of the total sources) to the CMD at $b = -3.0$ (46%). A more detailed comparison with the models is given in the next section.

5. Slicing the VVV bulge CMD

To study the bulge CMD in detail we divided the VVV bulge observations into 15 smaller areas, each comprising between 8 to 15 tiles ($\sim 12 - 22 \text{ deg}^2$, respectively), as marked in Fig. 2. This

analysis allows us to check by a quick view the main changes caused in the bulge stellar content by the differential reddening and extinction towards the Galactic centre.

Fig. 6 shows the 15 CMDs, with the areas numbered from #1 to #15, starting at the bottom-left corner. The mean stellar density and the central coordinates for each area are shown in the panels. Area #1 contains not only MW stars, but also the core of the Sagittarius dwarf galaxy, in a small proportion of $\sim 1 : 1000$ stars, according with Cseresnjcs et al. (2000).

The main differences between the CMDs occur at the Galactic latitude, while differences in Galactic longitude (which spans from $-10 \leq l \leq +10$) at the same b produces smaller changes. Thus, the central CMD in each line of panels of Fig. 6, corresponding to a given area along the bulge’s minor axis, is representative of its neighbours at higher longitudes. Fig. 7 highlights the region around the red clump giants for these central areas on the minor axis, from the outermost bulge (Area #2) to the Galactic centre region (Area #11). The figure shows the $K_s \times (J - K_s)$ CMDs and the $(J - H) \times (H - K_s)$ colour-colour diagrams (CCDs) for the given areas.

The RC of Area #2 is found to be double-peaked, with the brightest peak at $K_s = 12.75$ mag and the faintest one at $K_s = 13.45$ mag. The peaks appear with similar intensity to each other. The CCD of area #2 shows the RC as single-peaked, but displaced from the centre of a peanut-shaped structure. This can be interpreted as the sum of two closer distributions, as seen in the respective CMD.

The second row from the bottom of Fig. 6 shows the CMDs for areas #4, #5 and #6. These areas are moderately affected by extinction and reddening, and the main structures appear at similar colours and magnitudes as in the outermost region (areas #1 – #3). The RC becomes more prominent in relation to the MS and it is seen extended in magnitude. The CMD of Fig. 7 reveals a double-peaked structure, but now the farther RC (the fainter one, $K_s = 13.40$) is stronger than the closest one (the brighter, $K_s = 12.95$), compared with area #2, where the peaks show similar intensity. The peaks are closer to each other compared to area #2, with $\Delta K_s = 0.45$, compared with $\Delta K_s = 0.70$ for the outermost bulge. The CCD of Area #5 shows a similar behaviour as area #2, with a peanut-shaped structure with a single maximum.

Areas #7, #8 and #9 are affected by reddening and extinction at different levels, and show the RC spread over a broader colour range. Because the star density increases, the unresolved stars contribute to increase the background brightness limit, with the faintest point sources ~ 0.5 mag brighter around the minor axis (area #8). The red giant branch is seen single in area #7, with the RC also single, but spreading along the reddening vector. In area #8 the RC, and even the RGB seems to be double in colour, but in a closer separation. This separation becomes larger in area #9. The inspection of Fig. 7 shows that the RC main peak for area #8 appears at $(J - K_s) \sim 1.05$ over an elongated structure reaching $(J - K_s) \sim 0.90$, but at similar magnitude ($K_s \sim 13.15$ mag). Its CCD shows similar behaviour, with a single peak over an elongated peanut structure.

The Galactic centre is sampled in areas #10, #11 and #12. These are harder to interpret, since they are strongly affected by reddening and extinction. The sky brightness is even higher around the minor axis, with the faintest objects seen at $K_s \sim 16.5$ mag in area #11. This is the reason for the magnitude colour cut applied in Fig. 2. All populations are seen to be much redder, with the RC spreading along the direction of the reddening vector. The RC has a main peak at $(J - K_s) \sim 1.50$, with a difference of $\Delta(J - K_s) \sim 0.8$ mag in relation to the outermost region.

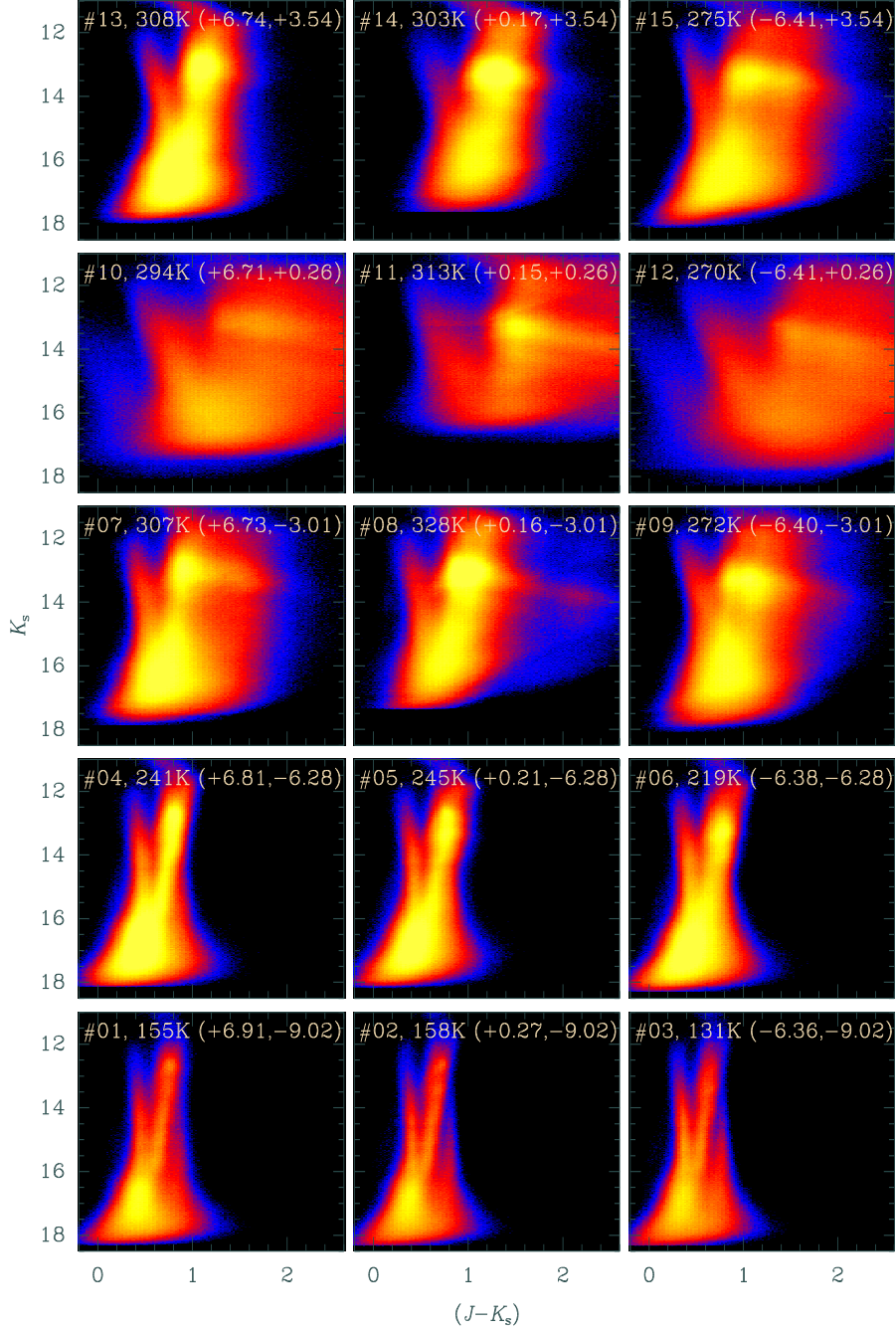


Fig. 6. CMDs for 15 different areas along the bulge as shown in Fig. 2. The areas were labelled from #01 (bottom-left corner) to #15 (top-right). The mean density of stellar sources (sources deg^{-2}) and the central coordinates (l, b) for each area are shown in the panels.

Areas #13, #14 and #15 are centred at $b = +3.54$ deg, and show a similar behaviour as seen for areas #07–09 (centred at $b = -3.01$ deg) but they are slightly less affected by extinction. At the minor axis (area #14) the RC stars are more prominent compared to the MSTO, while in the higher latitudes (areas #13 and #15) both RC and MSTO have similar strength.

5.1. The red clump giants

Owing to the well-defined absolute magnitude and colour (e.g., Alves 2000), and the well-understood dependence on age and metallicity (e.g., Salaris & Girardi 2002), clump giants have been used with success as distance indicators and calibrators in extinction studies (Paczynski & Stanek 1998; Alves et al. 2002; Minniti et al. 2011; Gonzalez et al. 2011, 2012). Our compari-

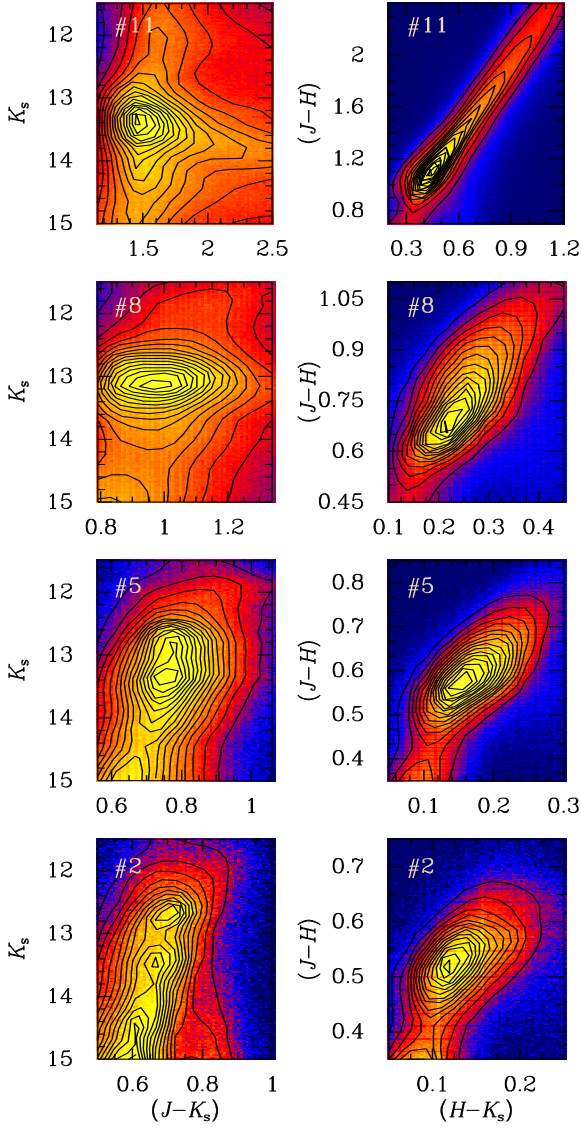


Fig. 7. Left-hand panels: $K_s \times (J - K_s)$ CMDs zoomed in the region around the Red Clump giants for areas #2, #5, #8 and #11, respectively, from the bottom to the top. The right-hand panels show the $(J - H) \times (H - K_s)$ CCDs for the same areas for all sources brighter than $K_s = 15$ mag.

son with models presented in Section 4 demonstrated that clump giants are the main population in the VVV bulge area, accounting for up to 46% of the total sources at $b = -3.0^\circ$. Even in the outer bulge, giants dominate at $K_s < 14$ mag.

Previous results have shown that the double RC in magnitude is the signature of the X-shaped MW bulge (e.g., McWilliam & Zoccali 2010; Nataf et al. 2010; Zoccali 2010; Saito et al. 2011b). These analyses focused on intermediate Galactic latitudes ($b \lesssim -6^\circ$), while Saito et al. (2011b) mapped the X-shape structure for the entire bulge within $3.5^\circ \leq |b| \leq 8.5^\circ$. The RC splits into two components for $|b| \gtrsim 5$, with the separation between the peaks increasing with the Galactic latitude, in agreement with the expectation of an X-shape structure seen almost edge-on, with the arms merging close to the Galactic centre. Our data are complementary to the previous results, and confirm the persistence of the X-shaped structure for $b \lesssim -8^\circ$, as seen in the CMDs of the outer bulge (areas #1-3). At area

#2 ($b \sim -9.0^\circ$) the double peak is seen very clearly in the VVV data, with the separation between peaks reaching $\Delta K_s \sim 0.7$ mag (see Fig. 7).

Combining data from regions where the RC appears with two peaks at different separations produces an elongated structure in magnitude for the final dataset. On the other hand, the differential reddening along the bulge, with up to $E(B - V) \sim 10$ at the Galactic centre (Gonzalez et al. 2012), causes the RC stars to spread along the reddening vector for more than $\Delta(J - K_s) \gtrsim 4$ mag. The combination of these effects contributes to create the complex shape of the RC seen in our CMD for the whole bulge.

5.2. The dwarf sequence

The CMDs of the outermost bulge regions (areas #1-3) show at the right-most side a well-defined sequence of relatively faint, $K_s \gtrsim 14$ mag, and red objects ($J - K_s \sim 0.7 - 0.9$ mag). The sequence merges with the disk sequence and the giant branch at lower magnitudes ($K_s \gtrsim 16$ mag), due to the large photometric errors in the bottom end of the CMD. The sequence is seen to be stronger towards negative longitudes, becoming more intense in the CMD for area #3. Interestingly, the sequence disappears at lower Galactic latitudes, and it is not visible in any other region of the VVV bulge.

The comparison with models presented in Section 4 shows the red dwarf sequence as seen in the CMDs for the area at $b = -9.5$ deg. The models reveal that the sequence is composed of main-sequence stars belonging to the thin disk (see Fig. 4). According to what is observed in CMDs for areas #4-6, the sequence is not detected at $b = -6.0^\circ$, because of the degeneracies introduced by crowding and differential reddening, which produce the red dwarf sequence overlaid with the bulge RGB.

We investigated the dwarf sequence in more detail and compared the colours of M-dwarfs provided by Hewett et al. (2006). Using colour transformations from UKIRT to the VISTA system and the mean extinction for the region, M-dwarfs from M1 to M6 coincide in colour with the main sequence, while later objects are slightly redder. Fig. 4 shows these objects in the CMD, assuming a distance modulus of $(m_{K_s} - M_{K_s}) = 7$ mag ($d \sim 250$ pc).

Interestingly, the red dwarf sequence is seen at $K_s \gtrsim 14$ mag, just beyond the limit of the 2MASS and DENIS photometry. This can explain why this was not noticed in previous near-IR studies. Deep CMDs such as those presented by Zoccali et al. (2003) should reveal the sequence, but their analysis was focused on fields at $b \sim 6.0^\circ$ where the red dwarf sequence is also absent in the VVV data, as described above. Lucas et al. (2008) reported a sequence with late K and M dwarfs in the UKIDSS GPS data, but at the opposite side of the Galaxy, at $l \sim 170 - 175$ deg. However, the sequence is not clearly distinguished from the RGB. The region at $b \sim 9.0 - 10$ deg seems to be ideal to survey these stars in the Galaxy, because the late dwarfs are seen in large numbers. The quality of the VVV photometry allows one to easily isolate the sequence using colour criteria. K and M dwarfs are particularly important in the planetary transit searches during the variability campaign of VVV, because their small size allows a better contrast with transits of low-mass planets (Saito et al. 2011a).

6. The CMD using reddening-free parameters

The bimodal colour distribution of the red clump can be interpreted as a reddening effect generated by the sampling of a large sky region with enough variation to produce the separation in

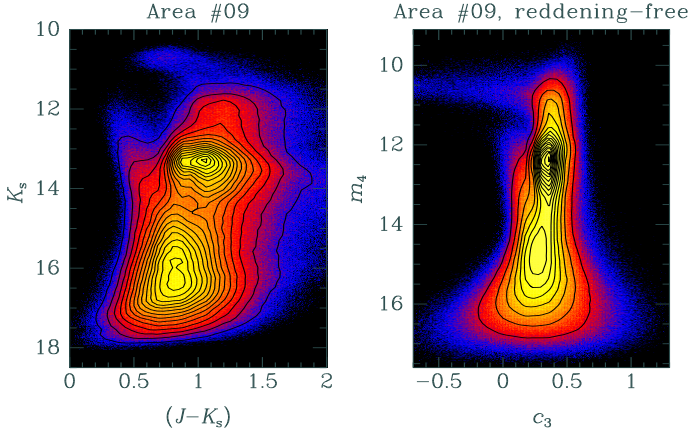


Fig. 8. $K_s \times (J - K_s)$ CMD for area #09 (left-hand panel) compared with the CMD made using reddening-free indices (right panel). The notation is similar to that presented in Fig. 3.

two components, and it can be also created by the observation of two distinct populations seen at the same line of sight.

In the VVV bulge area the RC spreading in colour, or even its splitting into a secondary peak, is seen across a large sky region, area #9 is the most drastic example. In this area the RC and even the RGB seems to be double in colour, with a separation of about $\Delta(J - K_s) \sim 0.2$ mag.

To test if the double RC is caused by differential reddening, we used reddening-free parameters provided by Catelan et al. (2011), based on the extinction law of Rieke & Lebofsky (1985) for the VISTA filters, namely m_4 and c_3 , defined as

$$m_4 \equiv K_s - 1.22(J - H), \quad (1)$$

$$c_3 \equiv (J - H) - 1.47(H - K_s). \quad (2)$$

Figure 8 shows the $K_s \times (J - K_s)$ CMD for area #9 (left panel) compared with CMD built using the reddening-free parameters $m_4 \times c_3$ for the same sources. It is very clear that the giant sequence becomes single, and the RC is seen with a very sharp single peak. Not only the giant sequence changed, but all structures are seen very concentrated (note the shorter colour range in the x-axis of the CMD built with the reddening-free parameters).

7. Conclusions

We presented the VVV colour-magnitude diagram of the Galactic bulge, the largest CMD ever published for a large homogeneous data set, with 84M+ stars. The interpretation of the CMD yields important information about the MW bulge, showing the fingerprint of its structure and content.

Stellar population synthesis models fit the data well, showing the predominance of main-sequence and giant stars in the outer bulge, which belong both to the bulge and halo. Thin- and thick-disk stars are also present in fewer numbers. In the inner bulge the CMD is dominated by bulge giants, which contribute up to 46% of the total sources at $b \sim -3^\circ$.

The analysis of the outermost bulge area reveals a well-defined sequence of late K and M dwarfs, seen at $(J - K_s) \sim 0.7 - 0.9$ mag and $K_s \gtrsim 14$ mag. These stars are particularly important in the planetary transit searches during the variability campaign of VVV.

The RC appears to be double in magnitude in the outer bulge region due to the X-shaped structure of the MW bulge, with the

separation between the peaks reaching $\Delta K_s = 0.70$ at $b \sim -9^\circ$. This result is complementary with previous analyses, and confirms the persistence of the X-shaped structure for $b \lesssim -8^\circ$. In contrast, in the inner part ($b \sim -3^\circ$) the RC appears to be spreading in colour, or even splitting into a secondary peak with a separation of $\Delta(J - K_s) \gtrsim 0.2$ mag (area #9). The use of reddening-free parameters confirmed that this last feature is caused by reddening effects.

The CMDs of the Galactic centre are harder to interpret because they are strongly affected by reddening and extinction. All populations are seen to be much redder, and the RC spreads along the direction of the reddening vector by $\Delta(J - K_s) \gtrsim 2.0$ mag.

Acknowledgements. We gratefully acknowledge use of data from the ESO Public Survey programme ID 179.B-2002 taken with the VISTA telescope, data products from the Cambridge Astronomical Survey Unit, and funding from the FONDAPE Center for Astrophysics 15010003, the BASAL CATA Center for Astrophysics and Associated Technologies PFB-06, the FONDECYT from CONICYT, and the Ministry for the Economy, Development, and Tourism's Programa Iniciativa Científica Milenio through grant P07-021-F, awarded to The Milky Way Millennium Nucleus. M.R. and D.M. are grateful for partial support by the National Science Foundation under Grant No. 1066293, and the hospitality of the Aspen Center for Physics. B.D. and B.B. acknowledge grants from CNPq/Brazil and FAPESP/Brazil. J.A. and M.C. acknowledge support by Proyecto Anillos ACT-86 and by Proyecto FONDECYT Regular No. 1110326. M.Z. acknowledges a fellowship from the John Simon Guggenheim Memorial Foundation and support by Proyecto FONDECYT Regular No. 1110393.

References

- Alcock, C., Allsman, R. A., Alves, D., et al. 1999, *ApJS*, 124, 171
- Alcock, C., Allsman, R. A., Alves, D. R., et al. 2000, *AJ*, 119, 2194
- Alves, D. R. 2000, *ApJ*, 539, 732
- Alves, D. R., Rejkuba, M., Minniti, D., & Cook, K. H. 2002, *ApJ*, 573, L51
- Cardelli, J. A., Clayton, G. C., & Mathis, J. S. 1989, *ApJ*, 345, 245
- Catelan, M., Minniti, D., Lucas, P. W., et al. 2011, *RR Lyrae Stars, Metal-Poor Stars, and the Galaxy*, 145
- Cseresnje, P., Alard, C., & Guibert, J. 2000, *A&A*, 357, 871
- Girardi, L., Groenewegen, M. A. T., Hatziminaoglou, E., & da Costa, L. 2005, *A&A*, 436, 895
- Gonzalez, O. A., Rejkuba, M., Minniti, D., et al. 2011, *A&A*, 534, L14
- Gonzalez, O. A., Rejkuba, M., Zoccali, M., et al. 2012, *arXiv:1204.4004*
- Hewett, P. C., Warren, S. J., Leggett, S. K., & Hodgkin, S. T. 2006, *MNRAS*, 367, 454
- Lucas, P. W., et al. 2008, *MNRAS*, 391, 136
- McWilliam, A., & Zoccali, M. 2010, *ApJ*, 724, 1491
- Minniti, D., et al. 2010, *New Astronomy*, 15, 433
- Minniti, D., Saito, R. K., Alonso-García, J., Lucas, P. W., & Hempel, M. 2011, *ApJ*, 733, L43
- Nataf, D. M., Udalski, A., Gould, A., Fouqué, P., & Stanek, K. Z. 2010, *ApJ*, 721, L28
- Nishiyama, S., Tamura, M., Hatano, H., et al. 2009, *ApJ*, 696, 1407
- Paczynski, B., & Stanek, K. Z. 1998, *ApJ*, 494, L219
- Rieke, G. H., & Lebofsky, M. J. 1985, *ApJ*, 288, 618
- Robin, A. C., Reylé, C., Derrière, S., & Picaud, S. 2003, *A&A*, 409, 523
- Robin, A. C., Marshall, D. J., Schultheis, M., & Reylé, C. 2012, *A&A*, 538, A106
- Saito, R. K., Minniti, D., Dékány, I., et al. 2011, *Revista Mexicana de Astronomía y Astrofísica Conference Series*, 40, 221
- Saito, R. K., Zoccali, M., McWilliam, A., et al. 2011, *AJ*, 142, 76
- Saito, R. K., Hempel, M., Minniti, D., et al. 2012, *A&A*, 537, A107
- Salaris, M., & Girardi, L. 2002, *MNRAS*, 337, 332
- Skrutskie, M. F., et al. 2006, *AJ*, 131, 1163
- Udalski, A., Szymanski, M., Kaluzny, J., Kubiak, M., & Mateo, M. 1993, *Acta Astron.*, 43, 69
- Zoccali, M., Hill, V., Lecœur, A., et al. 2008, *A&A*, 486, 177
- Zoccali, M., Renzini, A., Ortolani, S., et al. 2003, *A&A*, 399, 931
- Zoccali, M. 2010, *IAU Symposium*, 265, 271